Eur. Phys. J. A **28**, 237–243 (2006)
DOI 10.1140/epja/i2006-10026-8

THE EUROPEAN PHYSICAL JOURNAL A

String junction effects for forward and central baryon production in hadron-nucleus collisions

F. Bopp[a] and Yu.M. Shabelski[b]

Siegen University, Germany

Received: 24 March 2006 /
Published online: 20 June 2006 –
Communicated by Xiangdong Ji

Abstract. The process of baryon number transfer due to string junction propagation in rapidity space is considered. It leads to a significant effect in the net baryon production in pA collisions at mid-rapidities and an even more significant effect in the forward hemisphere for the cases of πA interactions. The results of numerical calculations in the framework of the Quark-Gluon String Model are in reasonable agreement with the data. Special consideration is given to Λ produced in $\pi^- A$ collisions extracted from the data of the WA89 Collaboration.

PACS. 25.75.Dw Particle and resonance production

1 Introduction

The Quark-Gluon String Model (QGSM) and the Dual Parton Model (DPM) are based on the Dual Topological Unitarization (DTU) and describe many features of high-energy production processes, both in hadron-nucleon and hadron-nucleus collisions [1–5] quite reasonably. In these models high-energy interactions proceed via the exchange of one or several pomerons and all elastic and inelastic processes result from cutting through or between pomerons [6] using the reggeon counting rules [7]. Each cut pomeron leads to the production of two strings of secondaries. Inclusive spectra of hadrons are in this way related to the corresponding fragmentation functions of quarks and diquarks at the end of the strings.

In the string models baryons are considered as configurations consisting of three strings attached to three valence quarks and connected in a point called "string junction" (SJ) [8–11]. String junctions are modelled as objects of nonperturbative QCD. It is very interesting to understand their role in the dynamics of high-energy hadronic interactions, in particular in the processes of baryon number transfer [12–16].

Important results connected with the transfer of baryon charge over long rapidity distances in string models were obtained in [17] and following papers [18,19]. In the present paper we consider such processes with transfers away from nuclear targets.

In nuclear targets these discussed transfers are enhanced due to two reasons. First, the usual production of secondaries (which can be considered as a background for string junction effects) in the beam fragmentation region is suppressed due to nuclear absorption [3,20–22]. Second, the probability of the baryon number transfer should be proportional to the number of inelastic interactions in the nuclear matter, $\langle\nu\rangle_{hA}$. In the case of baryon beams the SJ effects are the most visible in the central (mid-rapidity) region [17,18]. Most interesting for meson-nucleus collisions is the forward region. The rapidity range available for SJ effects is drastically expanded in this way.

2 Baryon as 3q + SJ system

In QCD hadrons are composite bound-state configurations built up from the quark $\psi_i(x), i = 1,\dots,N_c$ and gluon $G^\mu_a(x), a = 1,\dots,N_c^2-1$ fields. In the string models baryons are considered as configurations consisting of three strings attached to three valence quarks and connected in a point called the "string junction" (SJ) [8–11]. The correspondent wave function can be written as

$$B = \psi_i(x_1)\psi_j(x_2)\psi_k(x_3)J^{ijk}\,, \tag{1}$$

$$J^{ijk} = \Phi^i_{i'}(x_1,x)\Phi^j_{j'}(x_2,x)\Phi^k_{k'}(x_3,x)\epsilon^{i'j'k'}\,, \tag{2}$$

$$\Phi^i_{i'}(x_1,x) = \left[T\exp\left(g\int_{P(x_1,x)} A_\mu(z)\mathrm{d}z^\mu\right)\right]^i_{i'}\,. \tag{3}$$

[a] e-mail: Bopp@physik.uni-siegen.de
[b] *Permanent address:* Petersburg Nuclear Physics Institute, Gatchina, St. Petersburg, Russia;
e-mail: shabelsk@thd.pnpi.spb.ru

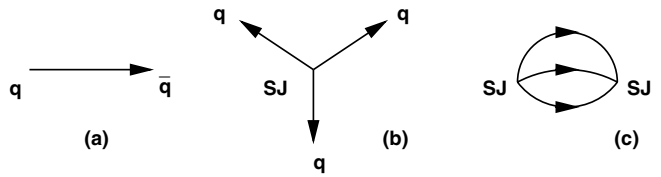

Fig. 1. Composite structure of a meson (a), a baryon (b) and a quarkless baryonium (c) in string models.

In the last equation $P(x_1, x)$ represents a path from x_1 to x which looks like an open string with ends in x_1 and x (see fig. 1b). Such baryon wave function can be defined as a "star" or "Y" shape, which is preferable [8,10], in comparison with "triangle" ("ring") or "$\triangle$" shape. The meson wave function

$$M = \psi_i(x_1)\Phi^i_{i'}(x_1, x_2)\psi^{i'}(x_2) \tag{4}$$

has the form of an "open string" with quark, respectively, antiquark on its end. Quarkless states (glueballs, see fig. 1c) are quite natural in this approach.

Such a picture leads to several phenomenological predictions. In the additive quark model the dynamic of the strings is attributed to its ends. This means that a meson consists of two constituent quarks as depicted in fig. 1a, and that a baryon consists of four constituent objects, three constituent quarks and a junction line (SJ), as it is shown in fig. 1b. The picture has an immediate consequence for the cross-sections. The ratio of nucleon-nucleon and meson-nucleon total cross-sections at high energies increases [23] in comparison with classical result [24] of $\sigma(N-N)/\sigma(\pi-N) = 3/2$. Accounting for the possibility of SJ interaction with a target one gets

$$\frac{\sigma(N-N)}{\sigma(\pi-N)} = \frac{3}{2} + \frac{\sigma(SJ-N)}{2\sigma(q-N)}\,, \tag{5}$$

where the additional term $\sigma(SJ-N)/(2\sigma(q-N))$ can be estimated [23] to be equal $1/5 \pm 1/7$. This correction results in better agreement [25] with experimental data.

Flavor-dependent quark antiquark annihilation will introduce corrections to this simple picture. The SJ annihilation in $B\bar{B}$ cross-section, σ_{ann}, is not necessarily the dominant effect. It is not equal to the difference $\Delta\sigma = \sigma^{tot}(B\bar{B}) - \sigma^{tot}(BB)$ [10].

The existence of SJ in a baryon structure changes the quark counting rules for reactions with large momenta transfer [12,13].

The reaction $\bar{p}p \to \bar{\Omega}\Omega$ can occur now without breaking the OZI rules. The ratio of $\bar{\Omega}/\Omega$ production for the collisions of non-strange hadrons is predicted to be smaller than unity [13] contrary to many models for multiparticle production. This prediction is in agreement with the experimental data [26] and their description in [17,18]. In the case of inclusive reactions the baryon number transfer to large rapidity distances in hadron-nucleon reactions can be explained by SJ diffusion [17].

In this paper we consider the effects of string junction for hadron-nucleus inelastic interactions.

3 Production of secondaries on nuclear targets in QGSM

As mentioned above, high-energy hadron-nucleon and hadron-nucleus interactions are considered in the QGSM and in DPM as proceeding via the exchange of one or several pomerons. As said, each pomeron corresponds to a cylindrical diagram, and thus, when cutting a pomeron two showers of secondaries are produced. The inclusive spectrum of secondaries is determined by the convolution of diquark, valence quark and sea quark distributions $u(x,n)$ in the incident particles and the fragmentation functions $G(z)$ of quarks and diquarks into secondary hadrons.

The diquark and quark distribution functions depend on the number n of cut pomerons in the considered diagram. In the following we use the formalism of QGSM.

In the case of a nucleon target the inclusive spectrum of a secondary hadron h has the form [1]:

$$\frac{x_E}{\sigma_{inel}}\frac{\mathrm{d}\sigma}{\mathrm{d}x} = \sum_{n=1}^{\infty} w_n \phi^h_n(x)\,, \tag{6}$$

where $x = 2p_\parallel/\sqrt{s}$ is the Feynman variable x_F and where $x_E = 2E/\sqrt{s}$.

The functions $\phi^h_n(x)$ determine the contribution of diagrams with n cut pomerons and w_n is the probability of this process. Here we neglect the contributions of diffraction dissociation processes which are comparatively small in most of the processes considered below. They can be accounted for separately [1,2].

In this paper we consider mainly the πA interactions, so we present the formulae for πp collisions

$$\begin{aligned}\phi^h_{\pi p}(x) = {} & f^h_{\bar{q}}(x_+, n) f^h_q(x_-, n) + f^h_q(x_+, n) f^h_{qq}(x_-, n) \\ & + 2(n-1) f^h_s(x_+, n) f^h_s(x_-, n)\,,\end{aligned} \tag{7}$$

where

$$x_\pm = \frac{1}{2}\left[\sqrt{4m_T^2/s + x^2} \pm x\right]\,, \tag{8}$$

where the transverse mass of the produced hadron is

$$m_T = \sqrt{m^2 + p_T^2}$$

and where f_{qq}, f_q and f_s correspond to the contributions of diquarks, valence quarks and sea quarks, respectively. They are determined by the convolution of the diquark and quark distributions with the fragmentation functions, *e.g.*,

$$f^h_{qq}(x_-, n) = \int_{x_-}^1 u_{qq}(x_1, n) \cdot G^h_{qq}(x_-/x_1)\ \mathrm{d}x_1\,. \tag{9}$$

In the case of nuclear targets we must consider the possibility of one or several pomeron cuts in each of the ν blobs of hadron-nucleon inelastic interactions as well as cuts between pomerons. For example, for a πA collision one of the cut pomerons links a valence antiquark and a

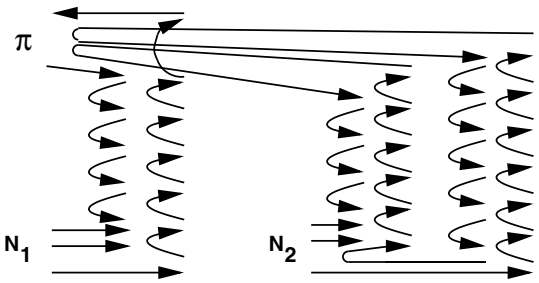

Fig. 2. One of the diagrams for inelastic interaction of an incident pion with two target nucleons N_1 and N_2 in a πA collission.

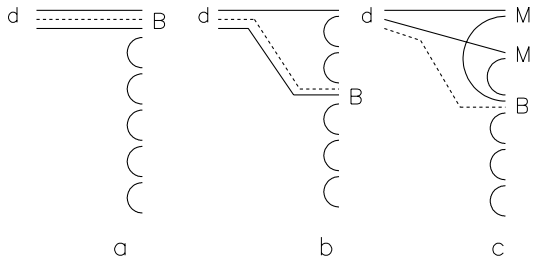

Fig. 3. QGSM diagrams describing the secondary baryon B production by diquark d: initial SJ together with two valence quarks and one sea quark (a), together with one valence quark and two sea quarks (b) and together with three sea quarks (c).

valence quark of the projectile pion with a valence quark and diquark of one target nucleon. The other pomerons link the sea quark-antiquark pairs of the projectile pion with diquarks and valence quarks of other target nucleons or with sea quark-antiquark pairs of the target.

For example, one of the diagram for inelastic interaction with two target nucleons is shown in fig. 2. In the blob of the πN_1 inelastic interaction one pomeron is cut, and in the blob of πN_2 interaction two pomerons are cut. It is essential to take into account every possible pomeron configuration and permutation on all diagrams. The process shown in fig. 2 satisfies the condition that the absorptive parts of hadron-nucleus amplitude are determined by the combinations of the absorptive parts of hadron-nucleon interactions.

In the case of inelastic interactions with ν target nucleons let n be the total number of cut pomerons in hA collisions ($n \geq \nu$) and n_i the number of cut pomerons connecting with the i-th target nucleon ($1 \leq n_i \leq n-\nu+1$). We define the relative weight of the contribution with n_i cut pomerons in every hN blob as $w_{n_i}^{hN}$. For the inclusive spectrum of the secondary hadron h produced in a πA collision we obtain [3]

$$\frac{x_E}{\sigma_{\pi A}^{prod}}\frac{\mathrm{d}\sigma}{\mathrm{d}x_F} = \sum_{\nu=1}^{A} V_{\pi A}^{(\nu)} \left\{ \sum_{n=\nu}^{\infty} \sum_{n_1=1}^{n-\nu+1} \cdots \sum_{n_\nu=1}^{n-\nu+1} \prod_{l=1}^{\nu} w_{n_l}^{\pi N} \times \left[f_{\bar{q}}^h(x_+,n) f_q^h(x_-,n_l) + f_q^h(x_+,n) f_{qq}^h(x_-,n_l) + \sum_{m=1}^{2n_l-2} f_s^h(x_+,n) f_s^h(x_-,n_m) \right] \right\}, \quad (10)$$

where $V_{pA}^{(\nu)}$ is the probability of "pure inelastic" (non-diffractive) interactions with ν target nucleons, and we should account for all possible pomeron permutation and for the difference in quark content of the protons and neutrons in the target.

In particular, the contribution of the diagram in fig. 2 to the inclusive spectrum is

$$\frac{x_E}{\sigma_{\pi A}^{prod}}\frac{\mathrm{d}\sigma}{\mathrm{d}x_F} = 2V_{\pi A}^{(2)} w_1^{\pi N_1} w_2^{\pi N_2} \left\{ f_{\bar{q}}^h(x_+,3) f_q^h(x_-,1) + f_q^h(x_+,3) f_{qq}^h(x_-,1) + f_s^h(x_+,n)[f_{qq}^h(x_-,2) + f_q^h(x_-,2) + 2f_s^h(x_-,2)] \right\}. \quad (11)$$

In the case of a nucleon beam the valence antiquark contributions of incident particle should be changed by the contribution of valence diquarks.

The diquark and quark distributions as well as the fragmentation functions are determined from Regge intercepts. Their expressions are given in appendix 1 of [17] (see also [18]).

According to [17,18] we account three possibilities that the secondary baryon can consist of the SJ together with two valence and one sea quarks (a), with one valence and two sea quarks (b) or with three sea quarks (c). They are shown in fig. 3.

The fraction of the incident baryon energy carried by the secondary baryon decreases from (a) to (c), whereas the mean rapidity gap between the incident and secondary baryon increases.

The processes shown in figs. 3a and b are the standard ones in QGSM and DPM. They determine the main contribution to the multiplicity of secondary baryons B in the fragmentation region. The most interesting for us at high energies is the case shown in fig. 3c, which leads to the difference in baryon and antibaryon production at rapidities far from the incident baryon (baryon charge diffusion in rapidity space). In the case of secondary baryon production with mass m in high-energy meson-nucleus collisions for positive (forward hemisphere) and not very small x_F the value $x_- \approx m_T^2/(x_F s)$ and the correspondent contribution to the target diquark fragmentation function (see eq. (9)) has the form

$$G_{SJ}^h(z) \sim \varepsilon z^{1-\alpha_{SJ}} . \quad (12)$$

Here ε is the relative suppression of the discussed contribution in comparison with the processes (a) and (b), and α_{SJ} is the intercept of the SJ Regge trajectory. In the present calculations we use the values $\varepsilon = 0.024$, $\alpha_{SJ} = 0.9$, and $a_N = 1.33$ as in [18]. Following the modern experimental data, we increase the portion of strange quarks in the sea, S/L [27,17] from $S/L = 0.2$ to $S/L = 0.32$.

To illustrate the expected effects of SJ contributions we present in fig. 4 the predicted inclusive cross-sections of $\pi^-\mathrm{Cu} \to \Lambda X$ and $\pi^-\mathrm{Cu} \to \Omega^- X$ reactions with (solid curves) and without (dashed curves) the SJ contributions of fig. 3c. These reactions were selected as the secondary baryons and the correspondent antibaryons $\bar{\Lambda}$ and $\overline{\Omega^+}$ have symmetrical quark states with respect to the incident

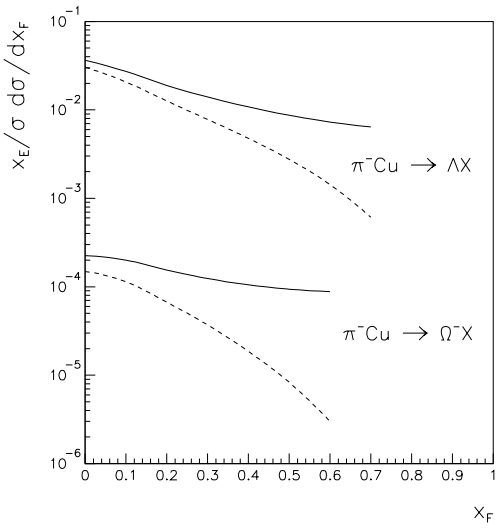

Fig. 4. The QGSM predictions for the inclusive cross-sections of Λ and Ω^- production in π^-Cu collisions at 400 GeV/c with (solid curves) and without (dashed curves) SJ contributions.

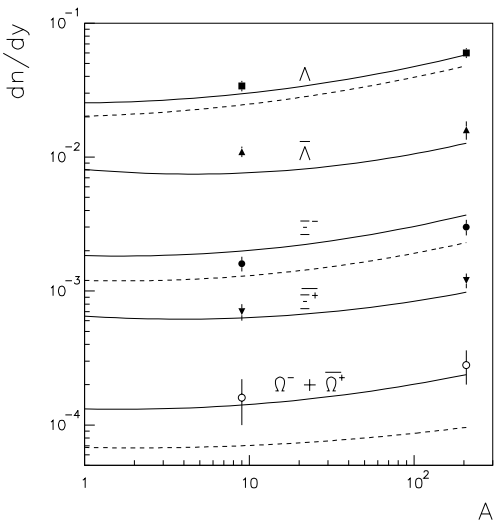

Fig. 5. Yields of Λ (closed squares), $\bar{\Lambda}$ (triangles), Ξ^- (points), $\overline{\Xi^+}$ (turned over triangles) and the sum $\Omega^- + \overline{\Omega^+}$ (stars) per unit of rapidity at central rapidity as a function of the target atomic weight for pA collisions at 158 GeV/c. QGSM predictions with SJ contribution are shown by solid curves and without SJ contribution by dashed curves.

π^-. So the SJ contribution equals to the difference between solid and dashed curves in fig. 4. It can be measured experimentally, as the difference in $\Lambda - \bar{\Lambda}$, or $\Omega^- - \overline{\Omega^+}$ production at high energies.

In general the SJ contribution shown in fig. 3c increases the inclusive cross-sections of Λ and Ω^- production. The spectra of antibaryons are not affected. However, numerically these effects are rather small, for example, the mean multiplicity of the secondary Λ in the forward hemisphere should increase about 15% which should be compensated by the correspondent decrease of the secondary nucleon multiplicity in the target region.

4 Comparison with the data

In fig. 5 we show the data [28] on the mid-rapidity inclusive densities, dn/dy, at $|y_{c.m.}| < 0.5$ of secondary Λ, $\bar{\Lambda}$, Ξ^-, $\overline{\Xi^+}$ and the sum $\Omega^- + \overline{\Omega^+}$ produced in pBe and pPb collisions at 158 GeV/c. These data are in reasonable agreement with the QGSM calculations and this agreement is better when taking the SJ contributions for secondary baryons into account.

In the case of pion-nucleus collisions at fixed target energies the SJ effects are more important. In fig. 6 we present the NA49 Collaboration data [29] on the x_F distributions of net protons $(p - \bar{p})$ produced in πp and πPb interactions at $\sqrt{s} = 17.2$ GeV. The beam π is determined in [29] as $(\pi^+ + \pi^-)/2$. The data are described rather well with the full model by taking the SJ diffusion into account (solid curves in fig. 6) and the variant without SJ contribution (dashed curves) underestimates the data several times at $x_F > 0.1$.

The experimental data of the WA89 Collaboration [30] on Λ, Ξ^- $\bar{\Lambda}$ and $\overline{\Xi^+}$ production from C and Cu targets by 345 GeV/c π^- beam are shown in fig. 7. The yields

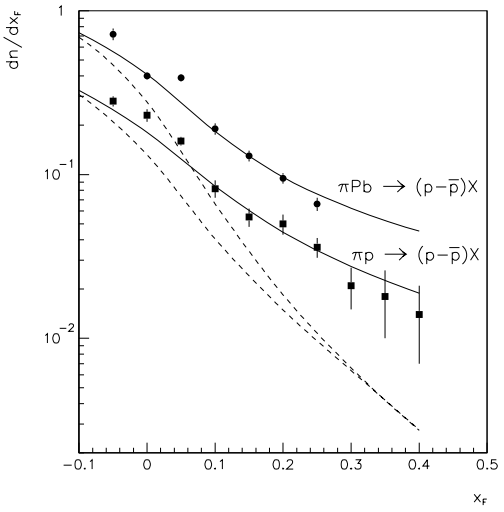

Fig. 6. Feynman-x distributions of net protons $(p - \bar{p})$ produced in πp (squares) and πPb (points) interactions at $\sqrt{s} =$ 17.2 GeV. Solid and dashed curves show the QGSM description with and without SJ contribution, respectively.

of secondary hyperons are in agreement with QGSM predictions accounting for the SJ contributions (solid curves in figs. 7a, b). The calculations without SJ contributions (dashed curves) are in disagreement with the data.

The yields of $\bar{\Lambda}$ and $\overline{\Xi^+}$ [30], which do not depend on SJ contribution, are shown in fig. 7c. These data are described by QGSM on the reasonable level.

The data presented in [30] allow one to calculate the asymmetries of secondary $\Lambda/\bar{\Lambda}$ production defined as

$$A_\Lambda = \frac{N_\Lambda - N_{\bar{\Lambda}}}{N_\Lambda + N_{\bar{\Lambda}}}\,. \tag{13}$$

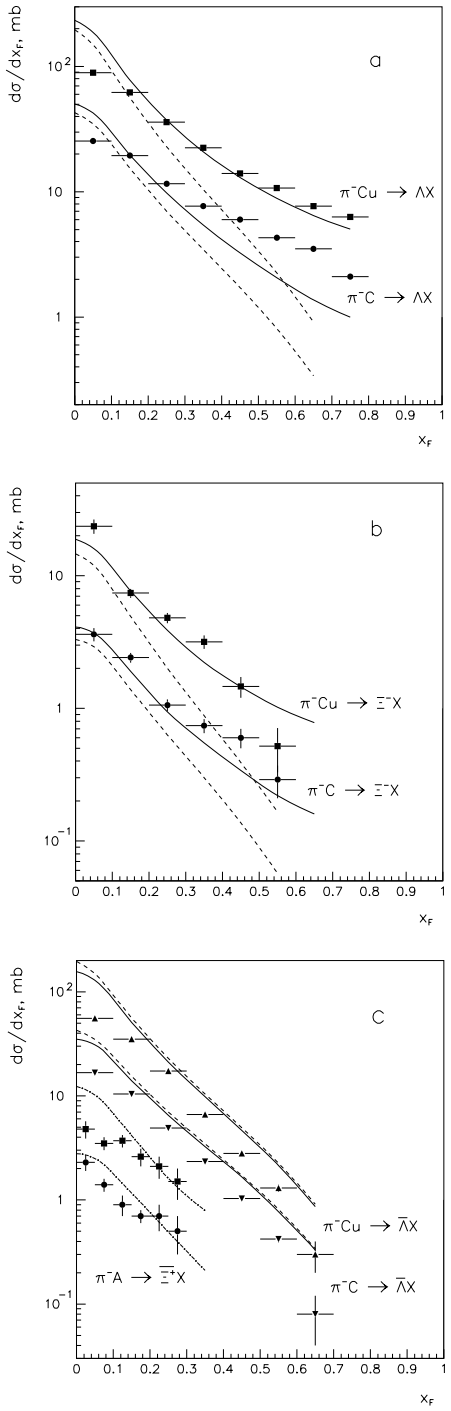

Fig. 7. Feynman-x distributions of secondary Λ (a), Ξ^- (b), $\bar{\Lambda}$ and $\overline{\Xi^+}$ (c) produced in π^-C and π^-Cu interactions at 345 GeV/c. Solid and dashed curves show the QGSM prediction for secondary hyperon spectra with and without SJ contribution. The QGSM predictions for antihyperon production in (c) are shown by dash-dotted curves (c).

They are presented in fig. 8a for the cases of π^-Cu (points) and π^-C (squares) interactions. The curves show the QGSM calculations for the cases of copper (dotted curve), carbon (dashed curve) and nucleon (solid curve) targets. We predict some A-dependence of the asymmetry for the beam fragmentation region. The agreement with the data

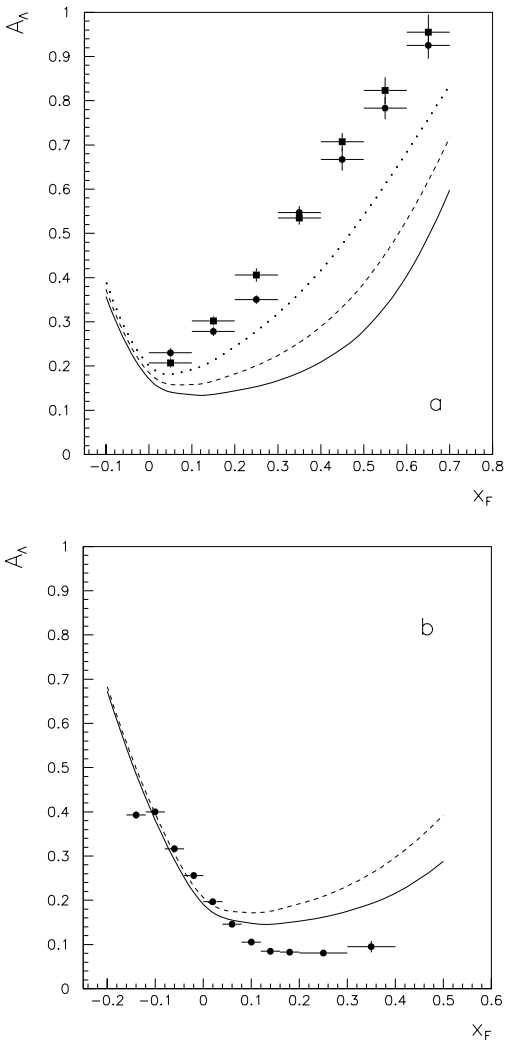

Fig. 8. The asymmetries of secondary $\Lambda/\bar{\Lambda}$ production in π^-C (squares) and π^-Cu (points) interactions at 345 GeV/c (a). The same asymmetries for $\pi^- A$ collisions at 250 GeV/c (b). Solid, dashed and dotted curves show the QGSM predictions for nucleon, carbon and copper targets, respectively.

is good in the central region, but the asymmetry is underestimated in the forward region.

In fig. 8b we present the data of [31] for the same asymmetry, eq. (13), obtained for π^- interactions with multifoil target with different atomic weights, see [31]. Here the QGSM predictions even for $\pi^- p$ interactions (solid curve), *i.e.* neglecting the A-dependence, overestimate the data at $x_F > 0.1$. In the central region, $|x_F| \leq 0.1$, our calculations are in agreement with the data of both [30] and [31] as well as of [26]. Here we predict the practical absence of A-dependence (or weak dependence) for $\Lambda/\bar{\Lambda}$ asymmetries, as was assumed in [17].

The comparison of the data shown in figs. 7a and c allows us to obtain the direct results for the SJ contribution to the hyperon production cross-section. Λ has the valence quark content uds, so the fast incident π^- ($\bar{u}d$) should fragment into secondary Λ and $\bar{\Lambda}$ with equal probabilities, *i.e.* the $\pi^- \to \Lambda$, respectively, $\pi^- \to \bar{\Lambda}$ fragmen-

Table 1. The values of the n parameter in eq. (14) obtained in [32] and [30] for Λ and $\bar{\Lambda}$ production in high-energy $\pi^- p$ and $\pi^- A$ collisions.

Reaction	n
$\pi^- p \to \Lambda$ [32]	2.0 ± 0.1
π^-C $\to \Lambda$ [30]	2.12 ± 0.02
π^-Cu $\to \Lambda$ [30]	2.71 ± 0.02
$\pi^- p \to \bar{\Lambda}$ [32]	2.0 ± 0.1
π^-C $\to \bar{\Lambda}$ [30]	5.23 ± 0.04
π^-Cu $\to \bar{\Lambda}$ [30]	5.53 ± 0.04

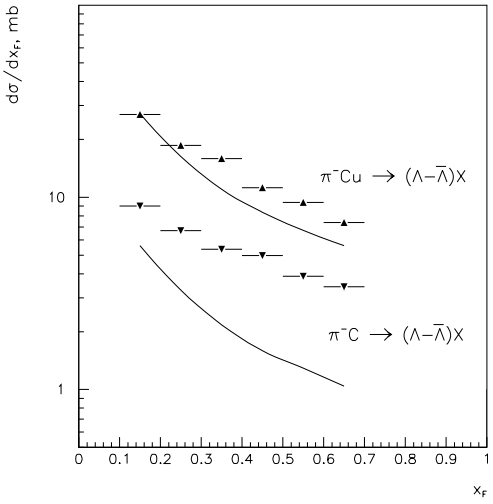

Fig. 9. The extracted SJ contributions to the spectra of Λ in $\pi^- A$ collisions at 345 GeV/c and their description by QGSM.

tation is flavour symmetrical, contrary, say, to the case of $\pi^- \to p$, respectively, $\pi^- \to \bar{p}$ fragmentation.

The contributions of the processes of figs. 3a and b are negligible at $x_F > 0.1$ and the difference in the spectra of secondary Λ and $\bar{\Lambda}$ determines the SJ contribution of the process shown in fig. 3c.

This difference is obtained to be rather large in [30] but very small in [32]. To show the disagreement between the data of [30] and [32] we present in table 1 the values of the parameter n for the parametrization

$$\mathrm{d}\sigma/\mathrm{d}x_F = C(1 - x_F)^n \,, \qquad (14)$$

which were obtained in [30] and [32] for secondary Λ and $\bar{\Lambda}$ production.

The values of n for the secondary Λ production obtained both in [30] and [32] on nucleon and on nuclear targets are in agreement with a natural weak A-dependence. The value of n slightly increases with A that demonstrates a well-known effect of nuclear absorption [3,20–22]. The values of n for $\bar{\Lambda}$ production obtained in [32] and [30] are absolutely different. The data of [32] show the absence or the very small contribution of SJ diffusion in the case of Λ and $\bar{\Lambda}$ production, in contradiction with other results, see for example [26].

It is possible to extract the SJ contribution from the experimental data of [30] only. The SJ contributions to the spectrum of secondary Λ in π^-Cu and π^-C collisions, obtained by such a way are presented in fig. 9.

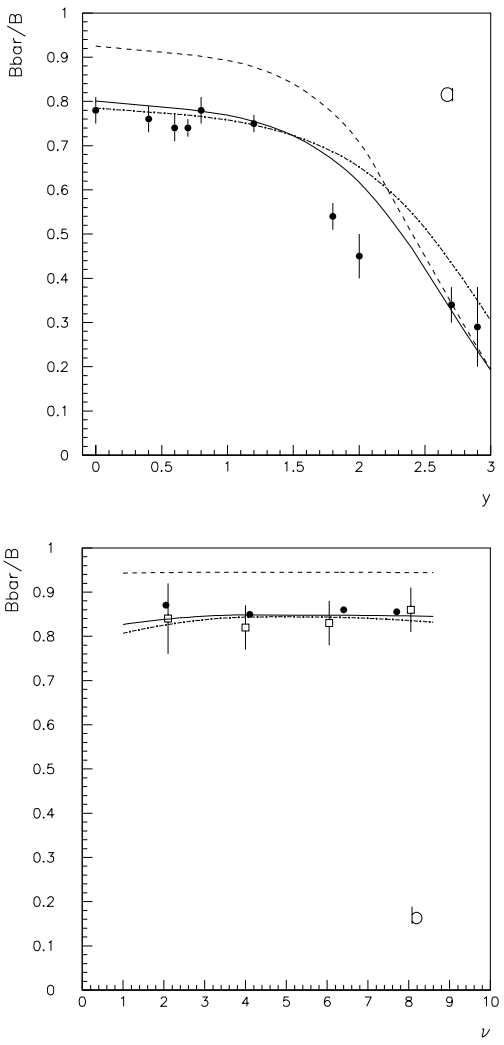

Fig. 10. The rapidity dependence of $\bar{p}/p$ ratios for pp collisions at $\sqrt{s} = 200$ GeV. Solid and dashed curves show the QGSM description with and without SJ contribution and the dash-dotted curve shows the QGSM predictions for the $\bar{\Lambda}/\Lambda$ ratio (a). The $\bar{p}/p$ ratio as a function of "centrality" for dAu collisions at $\sqrt{s} = 200$ GeV (open squares) together with the QGSM with SJ (solid curve) and without SJ (dashed curve) and with the DPMJET-III model (closed points) predictions. The QGSM predictions for the $\bar{\Lambda}/\Lambda$ ratio are shown by dash-dotted curves.

The x_F distributions of the Λ produced from copper target are in reasonable agreement with QGSM calculations, however, in the case of carbon target we obtain the disagreement coming mainly from the unsatisfactory description in fig. 7a and also from some overestimation of $\bar{\Lambda}$ production in fig. 7c. A reminder, the data [32] would lead to very small SJ contribution in this region way below the model.

There exists only a few data on secondary production in nucleon-nucleon and nucleon (deuteron) -nucleus collisions at RHIC energies. In fig. 10a we present the rapidity

(in c.m.) distribution of the ratio $\bar{p}/p$ in pp interactions at $\sqrt{s} = 200\,\mathrm{GeV}$ [33]. The QGSM calculation with the same SJ contribution (solid curve) is in reasonable agreement with the data, and the same calculations without SJ contributions (dashed curve) overestimate the discussed ratios.

In fig. 10b the dependence of $\bar{p}/p$ ratios at $|y_{c.m.}| = 0$ in dAu collisions is shown as a function of "centrality" at $\sqrt{s}$ = 200 GeV [34]. The experimental data are shown here by open squares and the QGSM predictions with SJ contribution by the solid curve which is very close to the constant. The calculations without SJ contribution (dashed curve) again lead to high values of $\bar{p}/p$ ratios. The close points in fig. 9b present the predictions of the DPMJET-III model [35] and they are in agreement with the data as well as with QGSM calculations. Dash-dotted curves in figs. 10a, b show the QGSM predictions for $\bar{\Lambda}/\Lambda$ ratios.

The predictions of several other models [36–38] are in some disagreement with the data of [34] (see fig. 4 in [34]). The extrapolation of the predictions of these models to $\nu = 1$ give the values of $\bar{p}/p$ in pp interactions larger than 0.9 that contradicts the data presented in fig. 10a.

5 Conclusions

We presented the role of string junction diffusion for the baryon charge transfer over large rapidity distances mainly for the case of collisions with nuclear targets. Without this contribution shown in fig. 3c the data for baryon/antibaryon yields and asymmetries are in disagreement with the data. The discussed string junction effects have A-dependences which are in general in agreement with the QGSM predictions (see, for example, fig. 6).

It is necessary to note that the existing experimental data are not enough for the determination of the SJ parameters with the needed accuracy. Some data are in disagreement with other ones, for example, the behaviour of $\bar{\Lambda}$ spectra at $x_F > 0$ obtained by [32] and [30], see table 1, and the $\Lambda/\bar{\Lambda}$ asymmetries in [30] and [31] which are presented in figs. 8a and b.

We are grateful to J. Ranft, R. Engel, G.H. Arakelyan, A.B. Kaidalov, L.N. Lipatov, O.I. Piskounova and A.A. Rostovtsev for useful discussions. This paper was supported by DFG grant GZ: 436 RUS 113/771/1-2 and, in part, by grants RSGSS-1124.2003.2 and PDD (CP) PST.CLG980287.

References

1. A.B. Kaidalov, K.A. Ter-Martirosyan, Yad. Fiz. **39**, 1545 (1984); **40**, 211 (1984); A.B. Kaidalov, O.I. Piskunova, Yad. Fiz. **41**, 1278 (1985).
2. A. Capella, U. Sukhatme, C.I. Tan, J. Tran Thanh Van, Phys. Rep. **236**, 225 (1994); A. Capella, J. Tran Thanh Van, Z. Phys. C **10**, 249 (1981).
3. A.B. Kaidalov, K.A. Ter-Martirosyan, Yu.M. Shabelski, Yad. Fiz. **43**, 1282 (1986).
4. Yu.M. Shabelski, Yad. Fiz. **44**, 186 (1986).
5. Yu.M. Shabelski, Nucl. Phys. Proc. Suppl. B **52**, 116 (1997).
6. V.A. Abramovski, V.N. Gribov, O.V. Kancheli, Yad. Fiz. **18**, 595 (1973).
7. A.B. Kaidalov, Sov. J. Nucl. Phys. **45**, 902 (1987); Yad. Fiz. **43**, 1282 (1986).
8. X. Artru, Nucl. Phys. B **85**, 442 (1975).
9. M. Imachi, S. Otsuki, F. Toyoda, Prog. Theor. Phys. **52**, 346 (1974); **54**, 280 (1976); **55**, 551 (1976).
10. G.C. Rossi, G. Veneziano, Nucl. Phys. B **123**, 507 (1977).
11. L. Montanet, G.C. Rossi, G. Veneziano, Phys. Rep. **63**, 149 (1980).
12. M. Imachi, S. Otsuki, F. Toyoda, Prog. Theor. Phys. **57**, 517 (1977).
13. H. Noda, Prog. Theor. Phys. **68**, 1406 (1982).
14. B.Z. Kopeliovich, B.G. Zakharov, Z. Phys. C **43**, 241 (1989); Fiz. Elem. Chast. At. Nucl. **22**, 140 (1991).
15. D. Kharzeev, Phys. Lett. B **378**, 238 (1996).
16. F. Bopp, hep-ph/0002190; hep-ph/0007229.
17. G.H. Arakelyan, A. Capella, A.B. Kaidalov, Yu.M. Shabelski, Eur. Phys. J. C **26**, 81 (2002); hep-ph/0103337.
18. F. Bopp, Yu.M. Shabelski, hep-ph/0406158; G.H. Arakelyan, C. Merino, Yu.M. Shabelski, hep-ph/0505100.
19. O.I. Piskounova, *Proceedings of the HERA-LHC Workshop*, edited by de Roeck *et al.*, DESY-PROC-2005-001, DESY (2005).
20. Yu.M. Shabelski, Nucl. Phys. B **132**, 116 (1978).
21. A. Capella, A. Krzywicki, Phys. Rev. D **18**, 3357 (1978).
22. V.V. Anisovich, Yu.M. Shabelski, V.M. Shekhter, Yad. Fiz. **28**, 1063 (1978); Nucl. Phys. B **133**, 116 (1978).
23. H. Kanada *et al.*, Prog. Theor. Phys. **59**, 2162 (1978).
24. E.M. Levin, L.L. Frankfurt, Pis'ma Zh. Eksp. Teor. Fiz. **2**, 105 (1965); H.J. Lipkin, F. Scheck, Phys. Rev. Lett. **16**, 71 (1966).
25. V.V. Anisovich, M.N. Kobrinsky, J. Njiri, Yu.M. Shabelski, Usp. Fiz. Nauk **144**, 553 (1984).
26. E769 Collaboration (E.M. Aitala *et al.*), hep-ex/0009016, Phys. Lett. B **469**, 9 (2000).
27. A. Capella, C.A. Salgado, Phys. Rev. C **60**, 054906 (1999).
28. WA97 Collaboration (F. Antinori *et al.*), Nucl. Phys. A **681**, 141c (2001).
29. NA49 Collaboration (H.G. Fischer), Nucl. Phys. A **715**, 118 (2003); hep-ex/0209043.
30. WA89 Collaboration (M.I. Adamovich *et al.*), Z. Phys. C **76**, 35 (1997); Eur. Phys. J. C **26**, 357 (2003).
31. E769 Collaboration (G.A. Alves *et al.*), Phys. Lett. B **559**, 179 (2003); hep-ex/0303027.
32. S. Mikocki *et al.*, Phys. Rev. D **34**, 42 (1986).
33. BRAHMS Collaboration (I.G. Bearden *et al.*), Phys. Lett. B **607**, 42 (2005); nucl-ex/0409002.
34. PHOBOS Collaboration (B.B. Back *et al.*), Phys. Rev. C **70**, 011901 (2004); nucl-ex/0309013.
35. F.W. Bopp, J. Ranft, R. Engel, S. Roesler, hep-ph/0505035.
36. M. Gyulassy, X.N. Wang, Comput. Phys. Commun. **83**, 307 (1994).
37. H. Sorge, Phys. Rev. C **52**, 3291 (1995).
38. Z.W. Lin *et al.*, Phys. Rev. C **64**, 011902 (2001); B. Zhang *et al.*, Phys. Rev. C **61**, 067901 (2000).